Permafrost extent sets drainage density in the Arctic

Joanmarie Del Vecchio (joanmarie@dartmouth.edu)[a, b, 1], Marisa Palucis (Marisa.C.Palucis@dartmouth.edu)[a], and Colin Meyer(Colin.R.Meyer@dartmouth.edu)[c]
[a] Department of Earth Sciences, Dartmouth College, Hanover, NH, USA; [b]Neukom Institute for Computational Science, Dartmouth College, Hanover, NH, USA; [c]Thayer School of Engineering, Dartmouth College, Hanover, NH, USA

Permafrost extent sets drainage density in the Arctic

Joanmarie Del Vecchio[a, b, 1], Marisa Palucis[a], and Colin Meyer[c]

[a]Department of Earth Sciences, Dartmouth College, Hanover, NH, USA; [b]Neukom Institute for Computational Science, Dartmouth College, Hanover, NH, USA; [c]Thayer School of Engineering, Dartmouth College, Hanover, NH, USA

This manuscript was compiled on May 2, 2023

Amplified warming of high latitudes and rapid thaw of frozen ground threatens permafrost carbon stocks. The presence of permafrost modulates water infiltration and flow, as well as sediment transport, on soil-mantled slopes, influencing the balance of advective fluvial processes to diffusive processes on hillslopes in ways that are different from temperate settings. These processes that shape permafrost landscapes also impact the carbon stored on soil-mantled hillslopes via temperature, saturation, slope stability such that carbon stocks and landscape morphometry should be closely linked. We studied >69,000 headwater basins between 25-90 °N to determine whether the thermal state of the soil sets the balance between hillslope and fluvial erosion processes, as evidenced by the density of the channel networks (i.e. drainage density) and the proportion of convex to concave topography (hillslopes and river valleys, respectively). Watersheds within permafrost regions have lower drainage densities than regions without permafrost, regardless of watershed glacial history, mean annual precipitation and relief. Independent of the dataset resolution and analysis method, we find evidence that advective fluvial processes are inhibited in permafrost landscapes compared to their temperate counterparts. Frozen soils likely inhibit channel development, and we predict that climate warming will lower incision thresholds to promote growth of the channel network in permafrost landscapes. By demonstrating how the balance of advective versus diffusive processes might shift with future warming, we gain insight into the mechanisms that shift these landscapes from sequestering to exporting carbon.

permafrost| drainage density | hydrology| soil carbon

Increasing Arctic air temperatures have led to intensification of the hydrologic cycle, reduction of spring snow cover and warming of near-surface permafrost (1). The amplified warming of high latitudes and potential degradation of permafrost landscapes and ecosystems threatens to disrupt global carbon fluxes via nascent warming feedbacks and thus global emission budgets (2, 3). The precise geomorphic mechanisms operating on permafrost landscapes as they evolve should determine whether they act as carbon sources (4) or sinks (5). However, the unique rheological and hydrological properties of permafrost landscapes that make their evolution sensitive to climate change complicate estimates of sediment and carbon fluxes in the midst of climate warming (6).

The size and shape of hillslopes and rivers elucidate the underlying processes moving sediment and water on a landscape. The spacing of ridges and valleys are set by the competition between diffusive soil transport, which smooths the landscape, and advective fluvial processes, which incise the landscape (7). In temperate landscapes, the length, curvature, and relief of hillslopes are a function of the pace and pattern of soil movement, which are controlled in part by climate and ecology (8–10). Topography can also elucidate how water moves through a landscape; the density and areal extent of the river network are set by the forces acting on the soil profile as it receives and transmits water from upslope and from precipitation (11, 12). As with soil transport, climate and ecology can control the formation of a fluvial network by setting the permeability structure and erodibility of soil as well as the overall volume of water transiting the system (11, 13). Drainage density is therefore influenced by "top-down" (climate) and "bottom-up" (geology and soil properties) processes that control when advection (fluvial incision) overcomes diffusion (soil creep).

The presence of permafrost modulates water infiltration, lateral flow, and sediment transport, on soil-mantled slopes. In permafrost landscapes, soil transport rates are set by the thermal and saturation state of the soil profile (14–16); likewise, tundra vegetation and permafrost soils mediate the flow of water in the subsurface (17). On some frozen hillslopes in the Arctic and Antarctic, the impermeable permafrost table routes surface and subsurface flow paths into zero-order geomorphic features called water tracks (18–22) (Figure 1). These linear zones of enhanced soil moisture can occur in the absence of well-defined channel valleys (18, 23) because timing of historically peak discharge from winter snow storage and spring melt (24) coincides with minimal ground thaw on hillslopes (18, 23, 24). Previous Arctic studies (18, 25, 26) indicated soil-mantled Arctic hillslopes experienced relatively limited channel development, but contrasting conceptual frameworks

Significance Statement

In permafrost landscapes, the competition between channel and hillslope processes directly impacts the amount of stored soil organic carbon. However, conceptual models disagree whether the presence of permafrost (and its subsequent thaw) lengthens or shortens channel networks on hillslopes, complicating predictions of carbon release under landscape disturbance. Our compilation of >69,000 watersheds showed that landscapes underlain by permafrost have fewer channels per watershed area (drainage density) and fewer river valleys compared to their temperate counterparts. Low drainage densities are likely supported by frozen ground, which is vulnerable to change with climate warming. Landscape positions that are vulnerable to geomorphic change may also be the locations of soil organic carbon that, if exposed, would impact greenhouse gas emission budgets.

JD designed study and wrote analysis code. JD, MP and CM contributed to writing of manuscript.

The authors declare no competing interests.

[1]To whom correspondence should be addressed. E-mail: joanmarie@dartmouth.edu

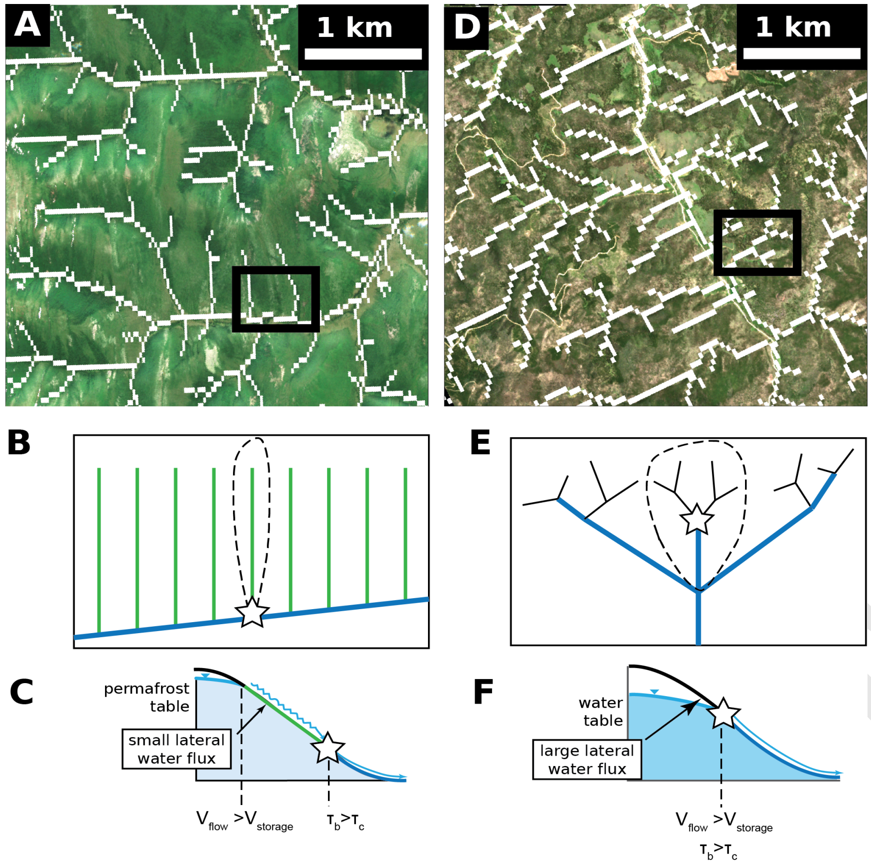

Fig. 1. Comparison between drainage densities and hydrogeomorphic configurations in comparable permafrost and temperate landscapes. (A) June 2022 visible imagery from a landscape in southeastern Russia underlain by continuous permafrost, mapped with the Hydrography90m stream segment data set (white; see text). The black box shows the area of the cartoon in Figure 1B. (B) Schematic of drainage network configurations in map view. The location of channel heads, where shear strength of flows surpass some threshold needed for incision and valley inception, is shown as a star. Water tracks (green) drain smaller, narrower areas (dashed line) than unfrozen low-order mountain streams. (C) In a cross-section of a hillslope, overland flow emerges higher up on the hillslope in permafrost landscapes, but incision within water tracks is limited by frozen ground and vegetation, which pushes the critical shear stress needed for incision downslope. (D) June 2022 imagery of a landscape in northwest U.S.A. with Hydrography90m dataset. (E-F) Channel networks are characterized by more branching, higher density of streams and channel heads closer to the ridgeline compared to the permafrost landscape. RGB imagery from Sentinel-2 MultiSpectral Instrument (ESA), accessed via Google Earth Engine.

hypothesize that hillslopes underlain by permafrost should exhibit longer channel networks due to the limited capacity for thawed soils to store water (27, 28). This competition between permafrost-modulated erodibility of channels and subsurface water storage, coupled with the importance of thaw-mediated sediment diffusivity, will determine whether permafrost landscapes exhibit a higher density of channels compared to their temperate counterparts.

The same top-down (climate) and bottom-up (geology) processes that control hillslope-channel coupling also influence the spatially variable soil organic carbon (SOC) (29, 30) such that carbon stocks and landscape morphometry should be closely linked (31). The dominance of diffusive processes over advective ones have the potential to sequester permafrost SOC (5), implying that soil-mantled permafrost landscapes with low drainage densities are likely to act as more efficient carbon sinks than those with more channels. Predicting how climate influences drainage density in polar region allows us to predict the balance of advective versus diffusive processes will shift with future warming, and thus how these landscapes may transition from sequestering to exporting carbon.

Our hypothesis is that, all other factors being equal, a landscape underlain by permafrost will have lower drainage density. Advection is limited by frozen ground and diffusion is enhanced by thaw-mediated creep. In order to account for the variety of bottom-up controls on drainage density independent of climate, we sampled >69,000 headwater catchments in the middle and high latitudes of the Northern Hemisphere to determine whether Arctic watersheds had significantly different drainage densities than otherwise-similar temperate watersheds. The large sample size allows us to account for lithologic controls on drainage density in the absence of constraints on substrate properties.

Results. When binned by relief and MAP, permafrost watersheds have lower drainage densities than their non-permafrost counterparts at a statistically significant level (Fig. 2A). This disparity is more pronounced for watersheds with lower MAP, such that arid permafrost watersheds have lower drainage densities than similarly arid unfrozen watersheds.Moreover, the extensiveness of the permafrost impacts drainage density monotonically; continuous and discontinuous permafrost promotes lower drainage density than isolated and sporadic permafrost, and less-extensive permafrost still promotes lower drainage density than landscapes without permafrost (Fig. 2B).

We found that this relationship is independent of recent glacial history (Fig. 2B), which would otherwise be a primary confounding variable considering the co-location of modern permafrost and ancient ice sheets in the Northern Hemisphere. Instead, for a given glacial history, more extensive permafrost consistently exhibits lower drainage density.

We investigated whether there is a correlation between mean annual temperature (MAT) and drainage density, as MAT exerts strong control on the thermal state of the near surface, which we hypothesize sets erodibility of the surface. Higher MATs are associated with higher drainage densities across all headwater catchments we studied regardless of permafrost presence (Fig. 3). MAT is closely related to mean annual precipitation (MAP) in our arid and semi-arid sites,

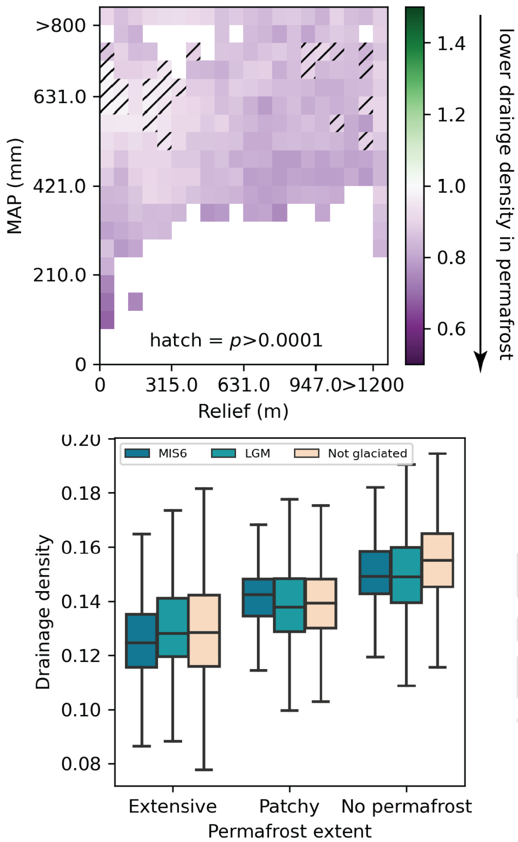

Fig. 2. Watershed drainage densities as function of location. (A) ratio of permafrost to non-permafrost drainage density for watersheds binned by relief and mean annual precipitation (MAP). Darker purple values indicate a lower ratio between the two settings (higher drainage density in permafrost watersheds). Hatch marks indicate bins in which a Mann-Whitney U test failed below p=1e-4 (see Materials and Methods). (B) Drainage density as a function of permafrost extent and glacial history. “Exensive” encompasses continuous and discontinuous permafrost, and “patchy” encompasses sporadic and isolated permafrost.

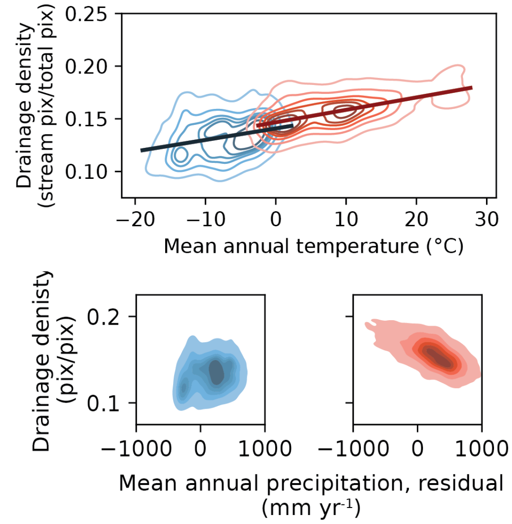

Fig. 3. Drainage density of studied watersheds as a function of their mean annual temperature (MAT) and mean annual precipitation (MAP). (A) Kernel density estimate plot for visualizing the distribution of drainage density for permafrost watersheds with MAT <2.5°C (shown in blue) and non-permafrost watersheds with MAT >2.5°C (shown in red). Linear regression fits are performed separately on the two datasets. (B-C) An ordinary least squares regression between MAT and MAP was performed to assign each watershed a residual MAP (see Supporting Information). KDE plots show density of residual values in permafrost (B) and non-permafrost (C) data with darker colors corresponding to high data density. Residual values for non-permafrost watersheds have a stronger relationship with drainage density, implying that variations in annual precipitation exert some control on drainage density for non-permafrost watersheds, but the relationship is weaker in permafrost watersheds

especially in the Arctic where higher MATs are generally associated with higher MAPs. To control for the covariation between MAT and MAP, we created a linear regression between MAT and MAP to calculate residual values for MAP. For watersheds not underlain by permafrost, particularly wet watersheds exhibit lower drainage densities than particularly dry watersheds; this trend is opposite and less pronounced for watersheds underlain by permafrost.

Landscape metrics derived from high resolution topographic data from 476 non-permafrost landscapes and 460 continuous permafrost landscapes corroborate these trends (Fig. 4A-B). Permafrost watersheds are characterized by a regime in which of intermediate flow accumulation ($10^3 - 10^4\ m^2$) occurs on planar to low-curvature slopes; this regime is absent from temperate watersheds, where positions in the landscape with these drainage areas are characterized by relatively high curvature values ($>10^{-4}\ m^{-1}$). Pixels in permafrost watersheds tend to exhibit more negative curvature values than in non-permafrost watersheds. Valleys form in watersheds underlain by permafrost at higher flow accumulations than in non-permafrost watersheds: the median drainage area for curvatures of 10^{-4} m^{-1} is over an order of magnitude higher in permafrost landscapes (46 x $10^3\ m^2$) than in non-permaforst landscapes (2.1 x $10^3\ m^2$).

Context from Literature. Abrahams and Ponczynski (32) observed that drainage density varied inversely with precipitation-evaporation ratios in semi-arid regions while it increased with increasing precipitation-evaporation ratios in humid environments, consistent with earlier work in the American West by Melton (33). This dynamic, in which climate zone dictates the

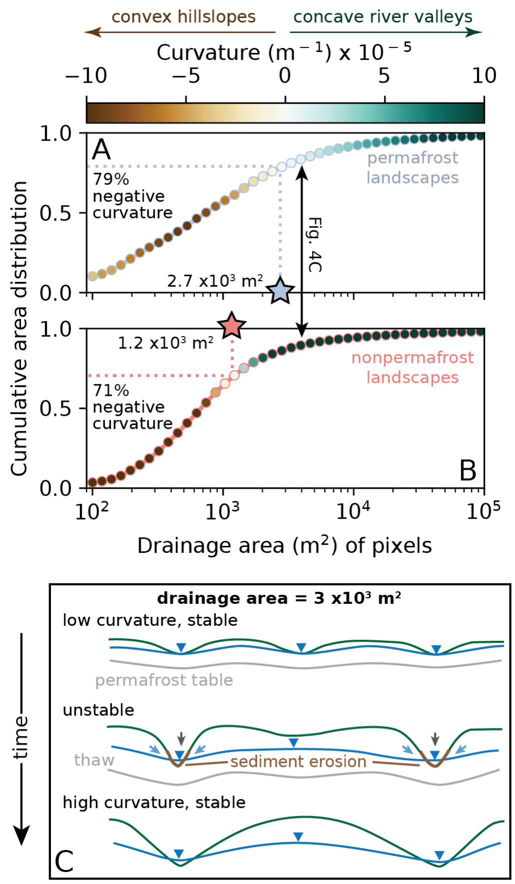

Fig. 4. Relationship between curvature, drainage area, and the use of permafrost and non-permafrost landscapes as a space-for-time substitution for the warming Arctic. (A-B) Median cumulative area distribution and curvatures as a function of drainage area in continuous permafrost (A) versus non-permafrost (B) landscapes. Stars indicate drainage areas associated with zero median curvature. Black arrow indicates drainage area and curvatures associated with cartoon in Figure 4C. (C) Hypothetical evolution of permafrost landscape undergoing warming. Under steady cold conditions, water tracks provide low-curvature flowpaths on permafrost hillslopes. With warming, water tracks coalesce as permafrost tables drop, leading to a positive feedback loop that concentrates subsurface flow, increases flow depth, drives cutting down of channels and carving valleys while drying up nearby water tracks and enhancing likelihood of inter-track erosion and carbon release. In the absence of permafrost, the system stabilizes with river valleys.

relationship between MAP and drainage density, was studied in numerical simulations (13, 34) and observed in high-resolution topography (35). Using data from sites in the mid-latitude USA, Sangireddy et al. (35) found that, in dry landscapes (<1050 mm/yr precipitation), drainage density decreases with increasing MAP and weakly decreases with increasing relief. Sangireddy et al. (35) also found that increasing vegetation cover results in decreased drainage density. Our study basins, which were filtered for a threshold vegetation index, fall within the arid and semi-arid classification of the Sangireddy et al. study and thus allow us to isolate the effects of temperature and precipitation on drainage density. Although we calculate drainage density on a coarser scale (and show the concordance of our method with traditional drainage density calculations; see Materials and Methods), our results show similar relationships for non-permafrost landscapes in which watersheds with higher MAP residuals exhibit lower drainage densities. In contrast, we find that permafrost watersheds exhibit increasing drainage density with increasing MAP despite falling within the arid and semi-arid precipitation classification, implying that different processes control the impact of rainfall on drainage density in the presence of frozen ground.

Proposed Mechanism. Arctic vegetation and the impermeable permafrost table mediate the flow of water on the surface and shallow subsurface, notably in water tracks (17, 19). We propose that the historical timing of peak runoff versus thaw conditions (24, 36), paired with water track ecogeomorphology (21, 37), results in few low-order valleys carved into watersheds underlain by frozen ground, leading to the low drainage densities observed in basins in more extensive permafrost (Figure 1). Water tracks emerge at the surface or near-surface at hillslope locations with sufficient upslope water (snowmelt, rainfall, or thawed ground ice) to promote the coalescence of flowpaths slightly inset into the background hillslope surface but still underlain by permafrost. At sufficiently large upslope drainage areas ($>10^4$ m^2), these flowpaths have enough thermal and mechanical erosive energy to alter longer-wavelength changes in surface topography and the shape of the permafrost table. These water tracks occupy the topographic space in between a saturation and incision threshold (12), the latter of which is controlled by the thermal state of the soil and the root strength of vegetation. The density of water tracks across a hillslope is likely controlled by constraints on lateral flowpaths into tracks (38), thermal subsidence, and surface processes.

Compared to their temperate counterparts with similar annual precipitation, watersheds with water tracks have many more distributed flowpaths that require a relatively high volume of water to do the geomorphic work of carving valleys that would promote subsequent advective processes. Whereas temperate landscapes' drainage density decreases with higher precipitation with the promotion of armoring vegetation (Figure 3 and (35)), any decrease in erodibility imparted by an increase in vegetation density (13) must be outcompeted by the effect of higher volumes of water in permafrost landscapes, producing the opposite trend in permafrost landscapes we observe in our data.

Warming in polar regions. The negative relationship between permafrost extent and drainage density forecasts the landscape changes that may accompany permafrost thaw under a warming climate. Previous temperature and precipitation conditions maintained frozen soil during peak snowmelt, inhibited incision of permafrost hillslopes. In the future, less precipitation will fall as snow and more precipitation will fall as rain across the Arctic (39, 40). Areas of hillslopes occupied by water tracks are likely to be geomorphically dynamic in the future; deeper and earlier thaw, combined with more rain and less snow, may cause sustained subsidence of the ground under water tracks (37). Inter-track water tables would respond by falling, potentially sapping shallower water tracks of interflow and lead flowpaths to coalesce (Figure 4C). Coalescing water tracks would lead to deeper flows and thus further promote incision into hillslopes and expansion of channel networks. Early thaw coincident with peak flow not only allows water to incise into mineral soil, but it allows for maximum leaching of mineral-associated carbon within organic horizons (41). The net carbon loss from this process is amplified if deeper thaw liberates old carbon for dissolution, transport, and photomineralization (42, 43). However, stable water tracks play an outsized role in emitting greenhouse gases in permafrost watersheds (44), such that the net carbon flux from their evolution to channels will depend on the magnitude of SOC loss due to erosion.

Materials and Methods

Data collection. We used the WWF HydroSHEDS Level 10 Basins dataset (45) hosted on Google Earth Engine to locate all headwater basins (defined as having no upstream contributing basin) between 23.5° and 90° N latitude. We further filtered this dataset to find soil-mantled watersheds by only selecting watersheds with average annual normalized difference vegetation index (NDVI) > 0.60, using each pixel's annual maximum NDVI for the year 2021 as measured by MODIS's 250 m Terra NDVI product (MOD13A1 v061). We masked the NDVI product by the MODIS water mask product (MOD44W v006). For remaining basins we extracted mean annual temperature (MAT) and mean annual precipitation (MAP) as reported by WorldClim BIO variables v1 (46), covering data between 1960-1991. Because most Arctic watersheds had MAP < 1000 mm/yr and MAP <1050 mm/yr was found to be the boundary of the inflection point in Sangireddy et al. (35), we eliminated watersheds with >1000 mm/yr precipitation. We calculated basin relief by subtracting the highest and lowest elevations within the watershed of digital elevation models created by NASA's Shuttle Ray Topography Mission (SRTM) for 25°-60° and ArcticDEM for 60°-90° (47). We calculated drainage density using the Hydrography90m dataset (48), which was created with the MERIT Hydro digital elevation model (resolution 90 m at the equator) to derive a global network of 726 million stream segments with a minimal upstream contributing area of 0.05 km^2. We masked this dataset with the MODIS water mask and calculated drainage density as the proportion of pixels associated with stream segments to the total number of flow accumulation pixels in the watershed boundary. Once watershed attributes were determined from climate and satellite data, we intersected the centroids of watersheds with the Circum-Arctic Map of Permafrost and Ground Ice Conditions (49) to classify watersheds into categories of continuous, discontinuous, sporadic, isolated, and no permafrost.

Overall ratios. We divided our data into "permafrost" (n=31,974) and "no permafrost" (n=37,618) based on the ground ice extent map. We binned each watershed of each group into one of 20 bins for MAP (range 0-1000 mm/year) and relief (range 0-1200 m) for a total of 400 bins. For bins that contained at least 10 permafrost watersheds in each bin, we calculated the ratio of the mean drainage density of permafrost versus non-permafrost datasets for each data bin (higher drainage density in permafrost watersheds results in a ratio <1.0). To test the significance of the difference in ratios for each bin, we performed a Mann-Whitney U test using the Python package scipy (50) on the distributions of drainage density for permafrost and non-permafrost watersheds. The Mann-Whitney U test is a non-parametric test that does not presume a normal distribution between two populations and tests whether any sample of one population will be larger than any sample from the other population. We chose a threshold of $p < 10^{-4}$ and differentiate bins that did not pass this significance test with hatches.

Control of glacial history. To confirm that glacial history is not a confounding variable in our study, we intersected the centroids with a map of the extent of the Last Glacial Maximum (LGM) at 24 ka at MIS 6 at 190 ka (51) to determine whether watersheds of different permafrost extents fell within the LGM boundary (which we assumed also included the MIS 6 extent), the MIS 6 boundary only, or unglaciated. We also performed Mann-Whitney U tests on boxplot pairs between permafrost extent categories for each of the glacial histories; all distribution differences are significantly different below a threshold of $p < 10^{-4}$.

Control of mean annual temperature. We selected unglaciated watersheds in our dataset and separated those unglaciated sites into watersheds with (n=16,002) and without (n=23,220) permafrost. We eliminated permafrost watersheds with MAT > 2.5 C and non-permafrost watersheds with MAT < -2.5 C. We performed an ordinary least squares (OLS) regression between MAT and drainage density for each group of watersheds. To determine the role that MAP might play in the MAT-drainage density relationship, we performed an OLS regression between MAT and MAP for both datasets using the Python package statsmodel and calculated the difference between a site's actual MAP and the regression fit prediction (residual) for each watershed. We then regressed these precipitation residuals against drainage density (Figure 3).

High-resolution subset and comparison to other methods. Both the coarse resolution of the underlying MERIT Hydro digital elevation model (90 m) and the simplified approach to delineating channels by area thresholds are drawbacks to the use of Hydrography90m to calculate drainage density (48). To check whether our results are influenced by either of these factors, we selected a random subset of non-permafrost and continuous permafrost watersheds (500 each) that spanned the range of relief and MAP represented by the larger dataset. We limited the non-permafrost watersheds to the conterminous US in order to use the 10 m USGS 3DEP National Map Seamless (1/3 Arc-Second) dataset hosted on Google Earth Engine. We downloaded topographic data for each watershed boundary from the USGS dataset (non-permafrost) and used bilinear resampling to downscale the 2 m ArcticDEM dataset to 10 m for continuous permafrost watershed boundaries. We then used the LSDTopoTools software suite (52) to preprocess the DEMs (remove invalid data, fill sinks, remove dams) and calculate basic topographic metrics (see Supporting Info for algorithm parameters). We created flow accumulation rasters with the d-infinity algorithm (53) and calculated tangential curvature with a window of 100 m. We then used the DrEICH algorithm (54), which uses curvature and channel steepness thresholds to select channel heads, to create channel networks using constants $A_0 = 1.0$ and $m/n = 0.5$. We calculated drainage density with the same pixel-counting method as the Hydrography90m dataset and found that while watersheds calculated with the Hydrography90m dataset contained 7x the proportion of channel pixels as the DrEICH algorithm channels, the correspondence between the two drainage density metrics was generally good (r^2 from OLS regression=0.80; see Supporting Information). The mean of the residual values for this regression is < 0 in permafrost and > 0 in non-permafrost, meaning that on average, Hydrography90m overestimates permafrost drainage density compared to the DrEICH algorithm and underestimates drainage density in non-permafrost watersheds. We then performed the same comparison between non-permafrost and permafrost drainage densities binned by relief and MAP as described in the text and shown in Figure 2A and found all bins to exhibit lower drainage densities in continuous permafrost watersheds, with most bins exhibiting p values < 0.005 (see Supporting Information).

We used the topographic metrics calculated from the high resolution subset to asses the dominance of concavity (created by advection) and convexity (created by diffusion) across the landscape independent of channel delineation. For each watershed in the subsample we calculated a cumulative area distribution for flow accumulation (drainage area) binned by drainage areas of $10^2 - 10^5$ m^2 to determine the relative proportion of flow accumulation values in a watershed. We also found the median tangential curvature for each of these flow accumulation bins to determine the drainage area associated with a switch from convex hillslopes (negative tangential curvature) to concave river valleys (positive tangential curvature). For each type of permafrost extent, we calculated the median cumulative area distribution and tangential curvature for each drainage area bin.

Data, Materials, and Software Availability. All data used in this study are freely available from their original sources, and all codes used to analyze and visualize data can be found at https://doi.org/10.5281/zenodo.7884727

ACKNOWLEDGMENTS. JD supported by the Neukom Institute for Computational Science, Dartmouth College. CRM supported by NSF (#2012958), NASA (21-EPSCoR2021-0024), and the Army Research Office (#78811EG). MCP supported by NSF (OPP-ANS-2116471) and NASA (SSW-80NSSC19K0539). The authors thank S. Evans and J. Levy for useful discussions on water tracks. Thank you to Samapriya Roy of awesome-gee-community-catalog for curating the Hydrography90m layers for Google Earth Engine.

1. JE Box, et al., Key indicators of Arctic climate change: 1971–2017. *Environ. Res. Lett.* **14**, 045010 (2019) Publisher: IOP Publishing.
2. SM Natali, et al., Permafrost carbon feedbacks threaten global climate goals. *Proc. Natl. Acad. Sci.* **118**, e2100163118 (2021).
3. EA Schuur, et al., Climate change and the permafrost carbon feedback. *Nature* (2015).
4. M Turetsky, et al., Carbon release through abrupt permafrost thaw. *Nat. Geosci.* (2020) Publisher: Springer US.
5. E Shelef, et al., Large uncertainty in permafrost carbon stocks due to hillslope soil deposits. *Geophys. Res. Lett.* **44**, 6134–6144 (2017) ISBN: 1944-8007.
6. JC Rowland, et al., Arctic landscapes in transition: Responses to thawing permafrost. *Eos* (2010) ISBN: 0894192090303.
7. JT Perron, WE Dietrich, JW Kirchner, Controls on the spacing of first-order valleys. *J. Geophys. Res. Earth Surf.* **113**, 1–21 (2008).
8. JJ Roering, JT Perron, JW Kirchner, Functional relationships between denudation and hillslope form and relief. *Earth Planet. Sci. Lett.* **264**, 245–258 (2007).
9. FJ Clubb, SM Mudd, M Attal, DT Milodowski, SW Grieve, The relationship between drainage density, erosion rate, and hilltop curvature: Implications for sediment transport processes. *J. Geophys. Res. Earth Surf.* **121**, 1724–1745 (2016).
10. SWD Grieve, SM Mudd, MD Hurst, How long is a hillslope? *Earth Surf. Process. Landforms* **41**, 1039–1054 (2016) ISBN: 0197-9337.
11. DR Montgomery, WE Dietrich, A physically based model for the topographic control on shallow landsliding. *Water Resour. Res.* **30**, 1153–1171 (1994) ISBN: 0043-1397.
12. GE Tucker, RL Bras, Hillslope processes, drainage density, and landscape morphology. *Water Resour.* **34**, 2751–2764 (1998).
13. E Istanbulluoglu, RL Bras, Vegetation-modulated landscape evolution: Effects of vegetation on landscape processes, drainage density, and topography. *J. Geophys. Res. Earth Surf.* **110**, 1–19 (2005) ISBN: 0148-0227.
14. MJ Kirkby, A Model for Variations in Gelifluction Rates with Temperature and Topography : Implications for Global Change. *Geografiska Annaler, Ser. A: Phys. Geogr.* **77**, 269–278 (1995).
15. N Matsuoka, Solifluction rates, processes and landforms: A global review. *Earth-Science Rev.* **55**, 107–134 (2001) ISBN: 0012-8252.
16. RS Anderson, SP Anderson, GE Tucker, Rock damage and regolith transport by frost: an example of climate modulation of the geomorphology of the critical zone. *Earth Surf. Process. Landforms* **38**, 299–316 (2013).
17. MA Walvoord, BL Kurylyk, Hydrologic impacts of thawing permafrost—a review. *Vadose Zone J.* **15** (2016).
18. JP Mcnamara, DL Kane, LD Hinzman, An analysis of an arctic channel network using a digital elevation model. *Geomorphology* **29**, 339–353 (1999).
19. M Luoto, New Insights into Factors Controlling Drainage Density in Subarctic Landscapes. *Arctic, Anarctic Alp. Res.* **39**, 117–126 (2007).
20. JS Levy, AG Fountain, MN Gooseff, KA Welch, WB Lyons, Water tracks and permafrost in Taylor Valley, Antarctica: Extensive and shallow groundwater connectivity in a cold desert ecosystem. *Bull. Geol. Soc. Am.* **123**, 2295–2311 (2011).
21. ED Trochim, MT Jorgenson, A Prakash, DL Kane, Geomorphic and biophysical factors affecting water tracks in northern Alaska. *Earth Space Sci.* pp. 123–141 (2016).
22. N Tananaev, Defrosting northern catchments: Fluvial effects of permafrost degradation. p. 20 (2022).
23. SJ Hastings, SA Luchessa, WC Oechel, JD Tenhunen, Standing biomass and production in water drainages of the foothills of the Philip Smith Mountains, Alaska. *Ecography* **12**, 304–311 (1989) _eprint: https://onlinelibrary.wiley.com/doi/pdf/10.1111/j.1600-0587.1989.tb00850.x.
24. A Bring, et al., Arctic terrestrial hydrology: A synthesis of processes, regional effects, and research challenges. *J. Geophys. Res. G: Biogeosciences* **121**, 621–649 (2016).
25. C Arp, et al., Drainage network structure and hydrologic behavior of three lake-rich watersheds on the arctic coastal plain, Alaska. *Arctic, Antarctic, Alp. Res.* **44**, 385–398 (2012).
26. JT Crawford, EH Stanley, EH Stanley, Distinct Fluvial Patterns of a Headwater Stream Network Underlain by Discontinuous Permafrost. *Arctic, Antarctic, Alp. Res.* **46**, 344–354 (2014) ISBN: 1938424646.
27. PW Bogaart, GE Tucker, JJD Vries, JJ de Vries, Channel network morphology and sediment dynamics under alternating periglacial and temperate regimes: A numerical simulation study. *Geomorphology* **54**, 257–277 (2003) ISBN: 0169-555X.
28. E Wohl, The challenges of channel heads. *Earth-Science Rev.* **185**, 649–664 (2018) Publisher: Elsevier.
29. K Yoo, R Amundson, AM Heimsath, WE Dietrich, Spatial patterns of soil organic carbon on hillslopes: Integrating geomorphic processes and the biological C cycle. *Geoderma* **130**, 47–65 (2006) ISBN: 00167061.
30. AA Berhe, et al., Persistence of soil organic matter in eroding versus depositional landform positions. *J. Geophys. Res. Biogeosciences* **117**, 1–16 (2012).
31. U Mishra, et al., Spatial heterogeneity and environmental predictors of permafrost region soil organic carbon stocks. *Sci. Adv.* **7**, eaaz5236 (2021).
32. AD Abrahams, JJ Ponczynski, Drainage density in relation to precipitation intensity in the U.S.A. *J. Hydrol.* **75**, 383–388 (1984).
33. M Melton, An analysis of the relations among elements of climate, surface properties, and geomorphology. *Tech. Rep. 11 Off. Nav. Res. Dep. Geol.* (1957).
34. DBG Collins, RL Bras, Climatic and ecological controls of equilibrium drainage density, relief, and channel concavity in dry lands: CLIMATE, DRAINAGE DENSITY, RELIEF, AND CONCAVITY. *Water Resour. Res.* **46** (2010).
35. H Sangireddy, RA Carothers, CP Stark, P Passalacqua, Controls of climate, topography, vegetation, and lithology on drainage density extracted from high resolution topography data. *J. Hydrol.* **537**, 271–282 (2016).
36. MA Walvoord, Development of perennial thaw zones in boreal hillslopes enhances potential mobilization of permafrost carbon. *Environ. Res. Lett.* p. 12 (2019).
37. SG Evans, SE Godsey, CR Rushlow, C Voss, Water Tracks Enhance Water Flow Above Permafrost in Upland Arctic Alaska Hillslopes. *J. Geophys. Res. Earth Surf.* **125**, 1–18 (2020).
38. CR Rushlow, AH Sawyer, CI Voss, SE Godsey, The influence of snow cover, air temperature, and groundwater flow on the active-layer thermal regime of Arctic hillslopes drained by water tracks. *Hydrogeol. J.* **28**, 2057–2069 (2020).
39. R Bintanja, O Andry, Towards a rain-dominated Arctic. *Nat. Clim. Chang.* **7**, 263–267 (2017).
40. L Landrum, MM Holland, Extremes become routine in an emerging new Arctic. *Nat. Clim. Chang.* **10**, 1108–1115 (2020) Publisher: Springer US.
41. C Hirst, et al., Seasonal Changes in Hydrology and Permafrost Degradation Control Mineral Element-Bound DOC Transport From Permafrost Soils to Streams. *Glob. Biogeochem. Cycles* **36** (2022).
42. JC Bowen, CP Ward, GW Kling, RM Cory, Arctic Amplification of Global Warming Strengthened by Sunlight Oxidation of Permafrost Carbon to CO2. *Geophys. Res. Lett.* **47**, e2020GL087085 (2020) _eprint: https://agupubs.onlinelibrary.wiley.com/doi/pdf/10.1029/2020GL087085.
43. MS Schwab, et al., An Abrupt Aging of Dissolved Organic Carbon in Large Arctic Rivers. *Geophys. Res. Lett.* **47**, e2020GL088823 (2020) _eprint: https://agupubs.onlinelibrary.wiley.com/doi/pdf/10.1029/2020GL088823.
44. TK Harms, G Rocher-Ros, SE Godsey, Emission of Greenhouse Gases From Water Tracks Draining Arctic Hillslopes. *J. Geophys. Res. Biogeosciences* **125** (2020).
45. B Lehner, G Grill, Global river hydrography and network routing: baseline data and new approaches to study the world's large river systems. *Hydrol. Process.* **27**, 2171–2186 (2013) _eprint: https://onlinelibrary.wiley.com/doi/pdf/10.1002/hyp.9740.
46. RJ Hijmans, SE Cameron, JL Parra, PG Jones, A Jarvis, Very high resolution interpolated climate surfaces for global land areas. *Int. J. Climatol. A J. Royal Meteorol. Soc.* **25**, 1965–1978 (2005).
47. C Porter, et al., ArcticDEM (2018).
48. G Amatulli, et al., Hydrography90m: a new high-resolution global hydrographic dataset. *Earth Syst. Sci. Data* **14**, 4525–4550 (2022) Publisher: Copernicus GmbH.
49. J Brown, KM Hinkel, FE Nelson, The circumpolar active layer monitoring (calm) program: Research designs and initial results. *Polar Geogr.* **24**, 166–258 (2000) Publisher: Taylor & Francis _eprint: https://doi.org/10.1080/10889370009377698.
50. P Virtanen, et al., SciPy 1.0: fundamental algorithms for scientific computing in Python. *Nat. Methods* **17**, 261–272 (2020) Number: 3 Publisher: Nature Publishing Group.
51. CL Batchelor, et al., The configuration of Northern Hemisphere ice sheets through the Quaternary. *Nat. Commun.* **10**, 1–10 (2019) Publisher: Springer US.
52. SM Mudd, et al., LSDTopoTools2 (2022).
53. DG Tarboton, A new method for the determination of flow directions and upslope areas in grid digital elevation models. *Water Resour. Res.* **33**, 309–319 (1997).
54. FJ Clubb, SM Mudd, DT Milodowski, MD Hurst, LJ Slater, Objective extraction of channel heads from high-resolution topographic data. *Water Resour. Res.* pp. 5375–5377 (2014) arXiv: 10.1002/2014WR016527 ISBN: 6176273099.

Supporting Information for

Permafrost extent sets drainage density in the Arctic

Joanmarie Del Vecchio, Marisa Palucis, Colin Meyer

Joanmarie Del Vecchio.
E-mail: joanmarie@dartmouth.edu

This PDF file includes:

Figs. S1 to S9
Tables S1 to S2
SI References

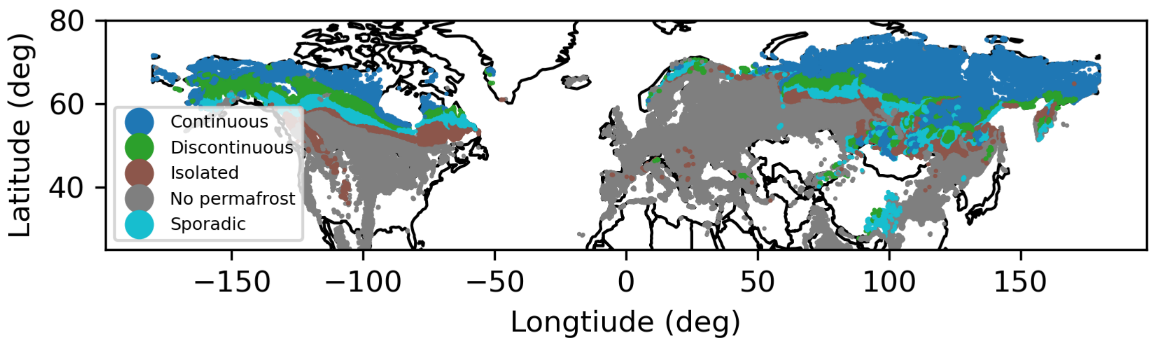

Fig. S1. Permafrost extent of watersheds in study (1)

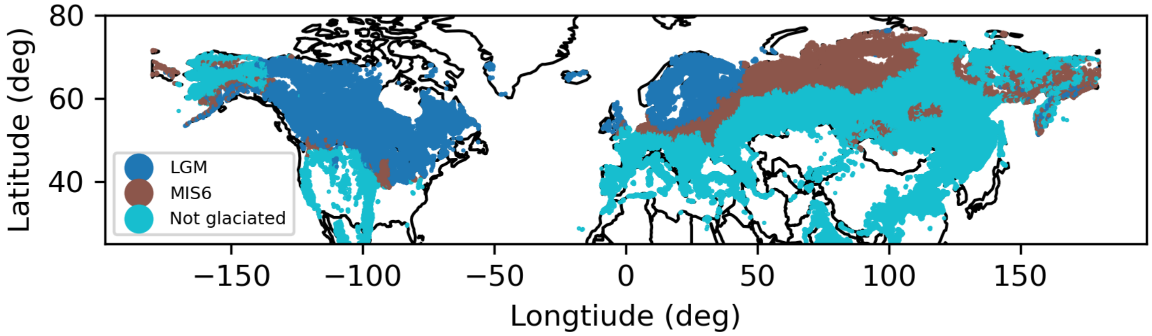

Fig. S2. Glacial history of watersheds in study (2)

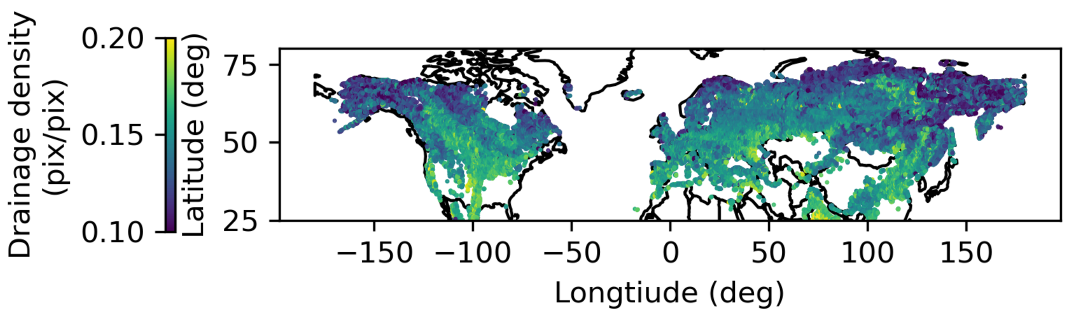

Fig. S3. Drainage density of watersheds in study

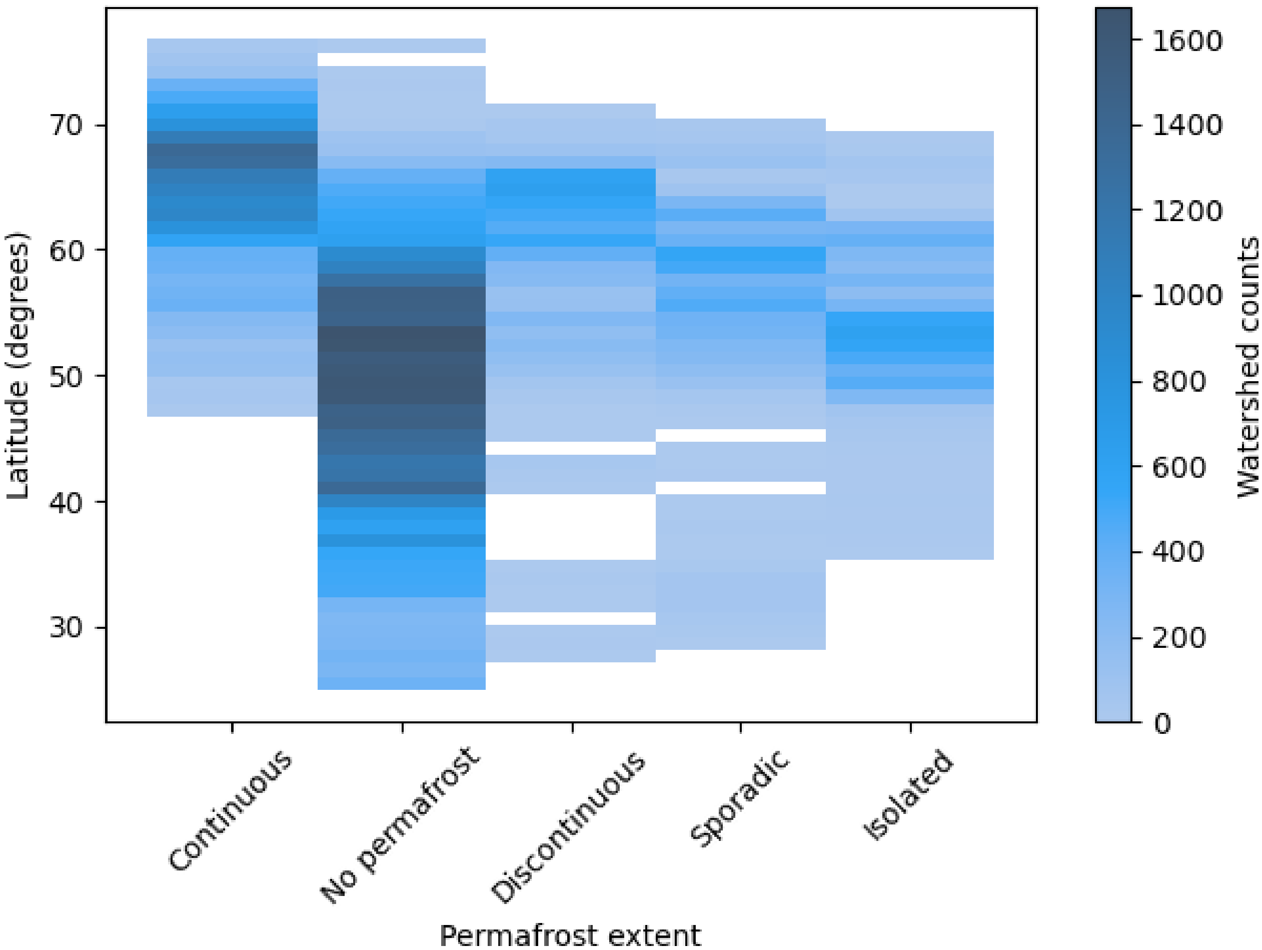

Fig. S4. Number of watersheds in each permafrost extent category by latitude

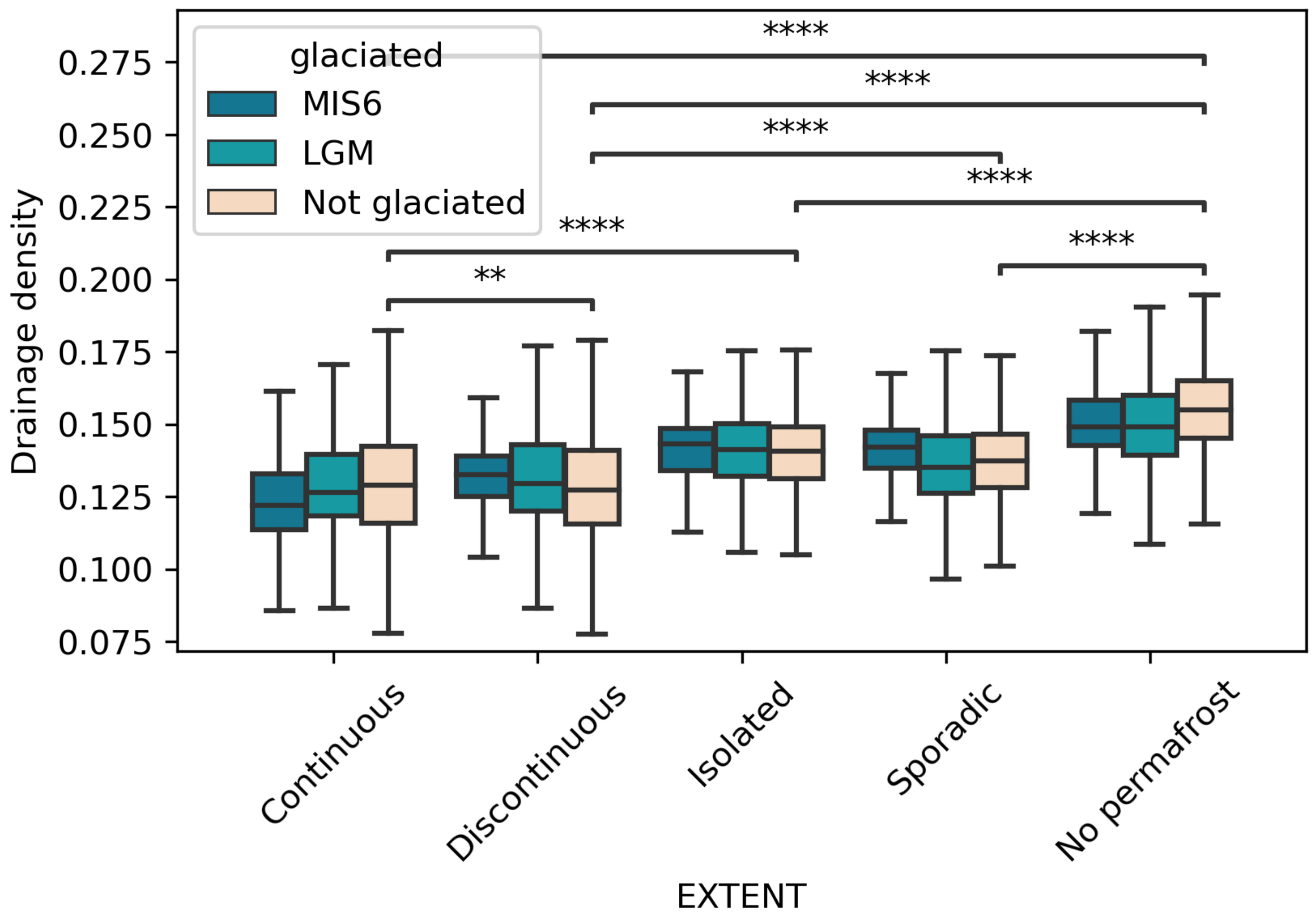

Fig. S5. Boxplot demonstrating distribution of drainage densities grouped by glacial history and permafrost extent types. The number of asterisks corresponds to the order of magnitude of the p-value from a Mann-Whitney U test (e.g. ** indicates 1.00e-03 < p <= 1.00e-02)

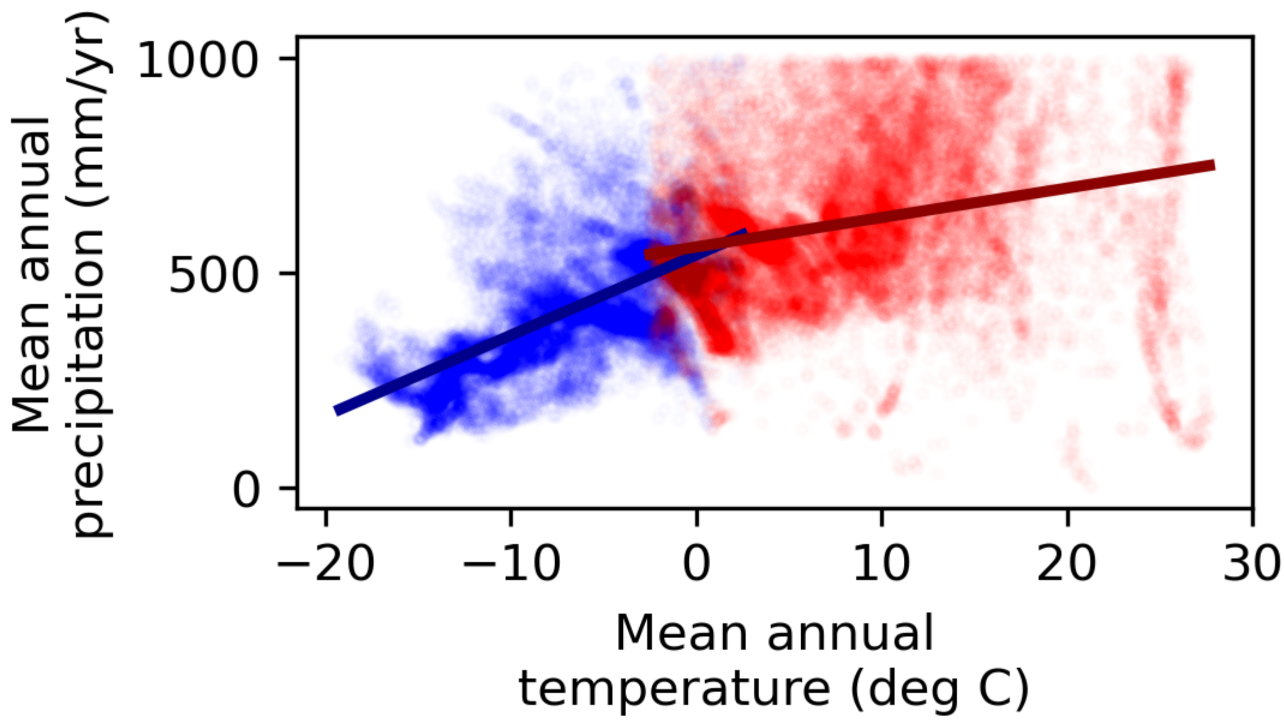

Fig. S6. Regression between mean annual temperature (MAT) and mean annual precipitation (MAP) (3) for permafrost (blue) and non-permafrost (red) watersheds used to calculate residuals for Figure 3B and C.

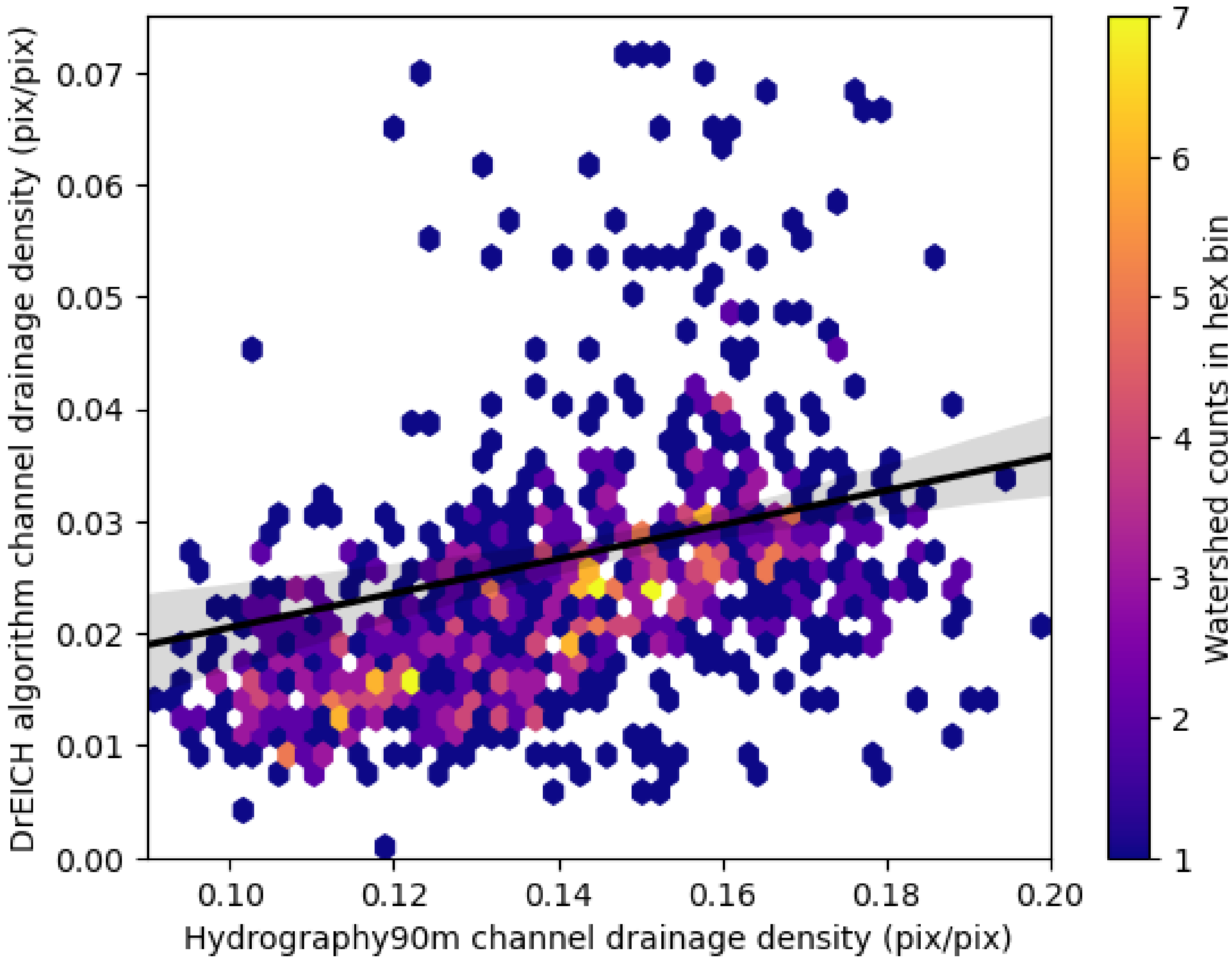

Fig. S7. Comparison of drainage density calculated the two sources of channel data (Hydrography90m (4) and DrEICH algorithm (5, 6))

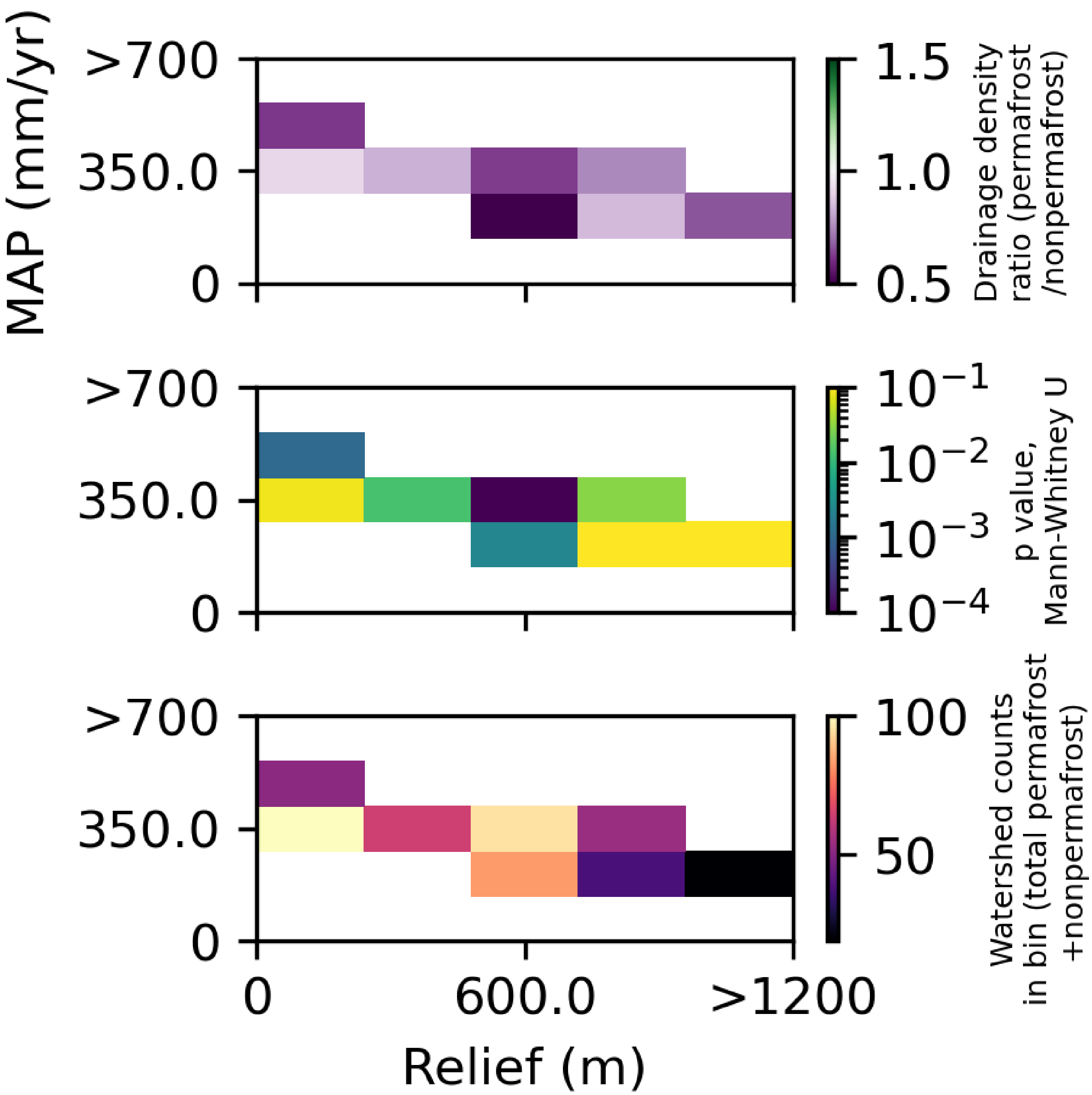

Fig. S8. Of the 936 subset watersheds from continuous permafrost and nonpermafrost, 504 had significant overlap in MAP-relief space and are compared here.

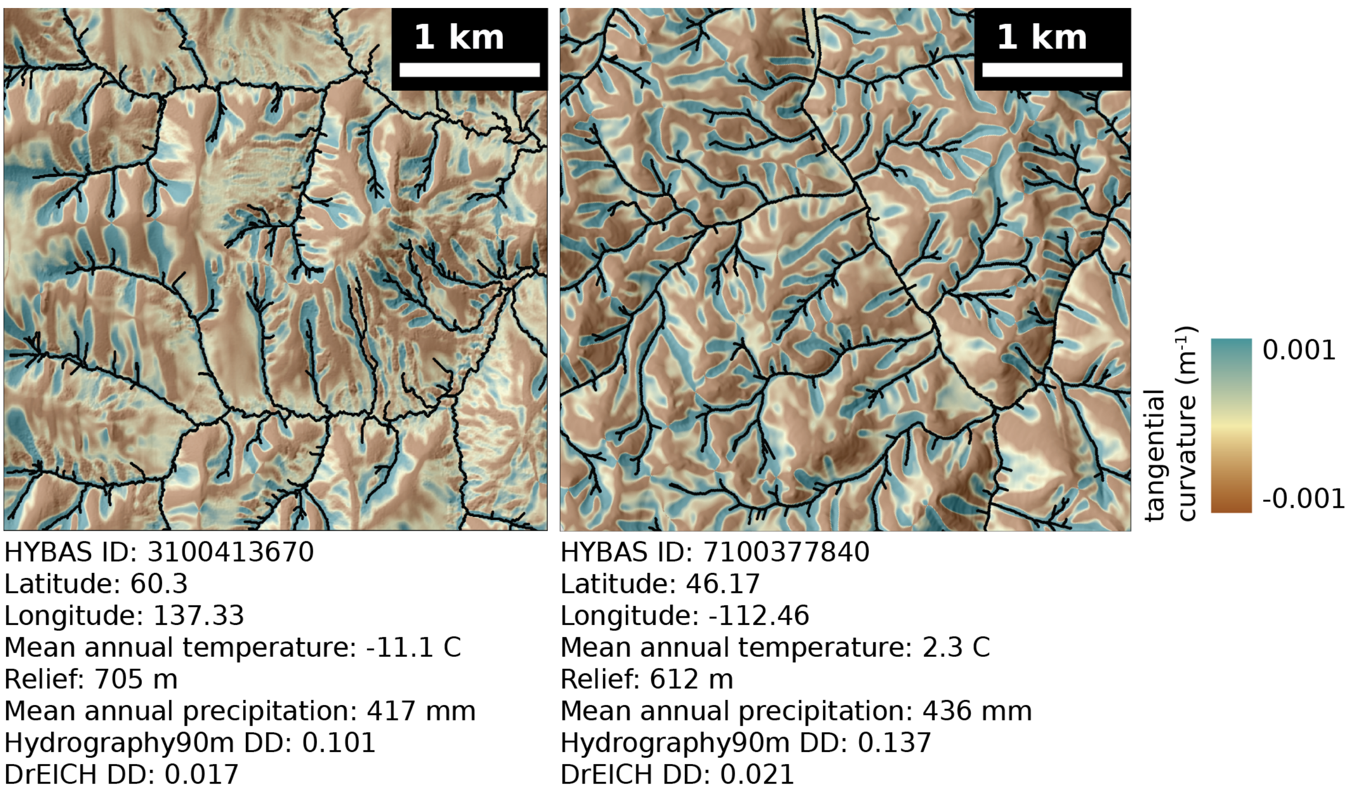

Fig. S9. Randomly selected watershed from continuous permafrost and non-permafrost landscapes (same as Figure 1A and 1D) with tangential curvature mapped with a hillshade and the DrEICH algorithm-generated channel networks.

Table S1. Number of watersheds grouped by both permafrost extent and glacial history categories

Permafrost extent	Glacial history	Watershed counts
Continuous	LGM	2004
	MIS6	4549
	Not glaciated	7923
Discontinuous	LGM	1911
	MIS6	1321
	Not glaciated	2772
Sporadic	LGM	2784
	MIS6	977
	Not glaciated	2104
Isolated	LGM	2177
	MIS6	338
	Not glaciated	3204
No permafrost	LGM	10645
	MIS6	3755
	Not glaciated	23220

Table S2. Parameters* for DEM preprocessing, curvature, and channel head algorithms for the LSDTopoTools (7) channel extraction algorithms

Parameter	value
`carve_before_fill`	True
`raster_is_filled`	False
`surface_fitting_radius` (m)	100
`threshold_contributing_pixels` (pixels)	5000
`A_0`	1.0
`m_over_n`	0.5
`pruning_drainage_area`	10
`connected_components_threshold`	10

*all other omitted parameters were set to defaults

References

1. J Brown, KM Hinkel, FE Nelson, The circumpolar active layer monitoring (calm) program: Research designs and initial results. *Polar Geogr.* **24**, 166–258 (2000) Publisher: Taylor & Francis _eprint: https://doi.org/10.1080/10889370009377698.
2. CL Batchelor, et al., The configuration of Northern Hemisphere ice sheets through the Quaternary. *Nat. Commun.* **10**, 1–10 (2019) Publisher: Springer US.
3. RJ Hijmans, SE Cameron, JL Parra, PG Jones, A Jarvis, Very high resolution interpolated climate surfaces for global land areas. *Int. J. Climatol. A J. Royal Meteorol. Soc.* **25**, 1965–1978 (2005).
4. G Amatulli, et al., Hydrography90m: a new high-resolution global hydrographic dataset. *Earth Syst. Sci. Data* **14**, 4525–4550 (2022) Publisher: Copernicus GmbH.
5. SM Mudd, et al., LSDTopoTools2 (2021).
6. FJ Clubb, SM Mudd, DT Milodowski, MD Hurst, LJ Slater, Objective extraction of channel heads from high-resolution topographic data. *Water Resour. Res.* pp. 5375–5377 (2014) arXiv: 10.1002/2014WR016527 ISBN: 6176273099.
7. SM Mudd, et al., LSDTopoTools2 (2022).